



Contents lists available at ScienceDirect

Arabian Journal of Chemistry

journal homepage: www.ksu.edu.sa

Original article

Efficient removal of Cr⁶⁺ by magnetically modified biochar from aqueous solution: Removal mechanism investigationChao Lv^a, Peng Liu^{b,*}^a School of Coal Engineering, Shanxi Datong University, Datong, Shanxi 037009, China^b School of Vanadium and Titanium, Panzhihua University, Panzhihua 617000, China

ARTICLE INFO

Keywords:

Magnetic biochar

Cr⁶⁺

Adsorption

Reduction

Economic feasibility

ABSTRACT

The magnetic biochar is prepared by one-pot method using waste wooden building formwork as feedstock in the existence of the FeCl₃ for Cr⁶⁺ removal from wastewater. Characterization analysis indicates that magnetic biochar exists Fe₃O₄ with specific surface area of the 333.89–496.35 m²/g, contributing to Cr⁶⁺ removal. Cr⁶⁺ removal process can be well analyzed by the Pseudo-second order and Hill models with adsorption capacity of 30.41 mg/g. The adsorption process analysis indicates that Cr⁶⁺ removal mechanism includes surface complexation, electrostatic attraction, reduction and pore filling. The influence of Fe²⁺ on Cr⁶⁺ removal is analyzed, indicating Fe²⁺ participation into Cr⁶⁺ removal by reduction. The magnetic biochar has excellent reusability after three cycles. The Cr⁶⁺ removal process is also investigated using column adsorption experiment, indicating that magnetic biochar has column adsorption amount of the 56.64 mg/g. The economic feasibility of the magnetic biochar is investigated and calculated with the production cost of \$2.48/1kg. The waste wooden building formwork is converted into the efficient magnetic biochar for Cr⁶⁺ removal from wastewater.

1. Introduction

The heavy metals in water bodies have posed serious threat to the human health and environment (Guo et al., 2024). Cr⁶⁺ is a common heavy metals in the groundwater, which has highly toxic, soluble and mobile in the environment (Qu et al., 2022). The wastewater containing Cr⁶⁺ is mainly produced from the tanneries, metal processing, electroplating and other basic industries (Xiao et al., 2024). The toxicity of the Cr⁶⁺ is much higher than the Cr³⁺, which can cause the skin cancer and respiratory problems for human beings (Hong et al., 2024). Excess Cr⁶⁺ in the ecosystem is not only harmful to the humans but also inhibits the growth and development of other organisms (Mao et al., 2024). The maximum limited Cr⁶⁺ concentration is 0.05 mg/L in drinking water (Cai et al., 2023). Therefore, removal Cr⁶⁺ from above industries wastewater is necessary.

In order to control the pollution of Cr⁶⁺ wastewater, several treatment methods such as electrochemical, membrane filtration and photocatalytic degradation have been used for Cr⁶⁺ wastewater treatment (Fu and Wang, 2011). However, compared with these costly and complex methods, adsorption is the common and efficient methods for Cr⁶⁺

removal from wastewater. Many adsorbents including activated carbon, clay mineral and biochar are used for Cr⁶⁺ removal from wastewater (Fu and Wang, 2011; Zhao et al., 2021; Zou et al., 2021). For sustainably and high efficient removing Cr⁶⁺ from wastewater, it can be found that it is essential for development of the low-cost adsorbents.

Biochar is produced at the temperature of 400–600 °C in the inert atmosphere, which is also the byproducts of biomass pyrolysis. The production cost of biochar is about \$448.78/t (Qin et al., 2023). Biochar can be an alternative for adsorptive elimination of Cr⁶⁺ as the result of its abundant functional groups and pore structure. Li et al. (2022) prepared the Landfill leachate sludge-based biochar for Cr⁶⁺ removal from wastewater, exhibiting adsorption capacity of 17.46 mg g⁻¹ (Li et al., 2022). Singh et al. (2022) prepared the biochar derived from Citrobacter freundii bacterial biochar for Cr⁶⁺ removal with adsorption capacity of 19.43 mg g⁻¹ (Singh et al., 2022). Mutabazi et al. 2024 prepared the peanut shell-derived biochar for Cr⁶⁺ wastewater purification with adsorption capacity of 16.67 mg g⁻¹ (Mutabazi et al., 2024). Amin et al. (2019) prepared marine Chlorella sp. Residue-based biochar for Cr⁶⁺ removal with adsorption amount of 15.94 mg g⁻¹ (Amin and Chetpatanondh, 2019). However, the above literatures only investigate the

Peer review under responsibility of King Saud University.

* Corresponding author.

E-mail address: liupeng22@pzh.edu.cn (P. Liu).<https://doi.org/10.1016/j.arabjc.2024.105943>

Received 8 May 2024; Accepted 26 July 2024

Available online 31 July 2024

1878-5352/© 2024 The Authors. Published by Elsevier B.V. on behalf of King Saud University. This is an open access article under the CC BY-NC-ND license (<http://creativecommons.org/licenses/by-nc-nd/4.0/>).

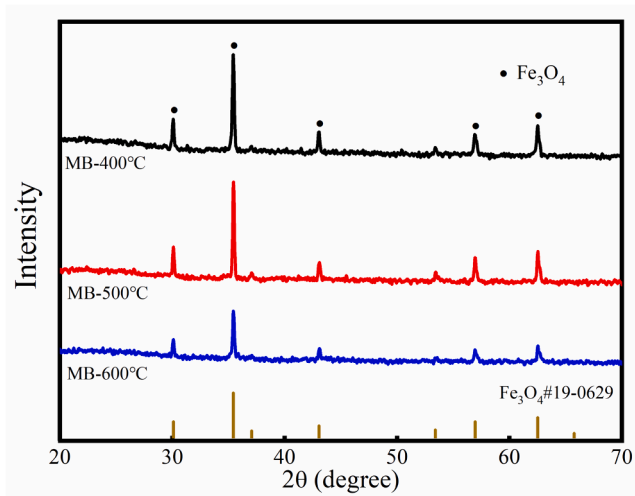


Fig. 1. XRD pattern of the magnetic biochar.

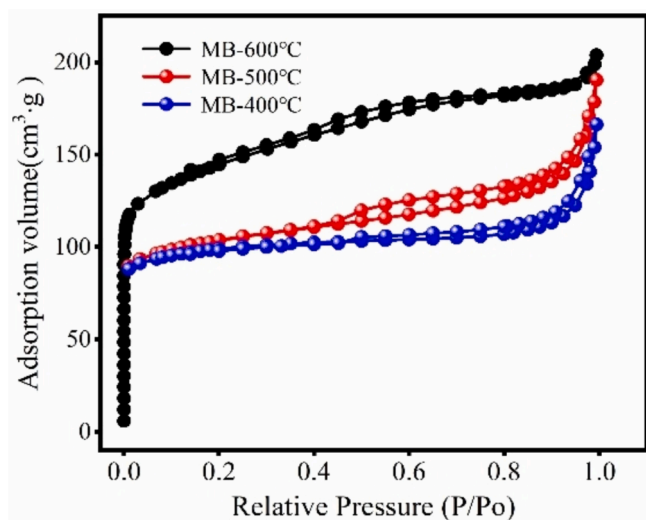


Fig. 2. N₂-adsorption/desorption isotherm of magnetic biochar.

Table 1
Pore structure of the magnetic biochar.

Item	Surface area (m ² /g)	Pore volume (cm ³ g ⁻¹)	Average pore size (nm)
MB-600 °C	496.35	0.32	2.54
MB-500 °C	350.73	0.29	3.36
MB-400 °C	333.89	0.26	3.08

Cr⁶⁺ adsorption performance of original biochar with modest adsorption capacity, which limits uptake ability for Cr⁶⁺ removal from wastewater.

There are many methods for modification biochar to improve its pore structure, chemical surface functional groups, etc for improvement of adsorption capacity. Combining Fe-based compounds such as Fe₃O₄, FeC₃ and zero-valent iron with biochar to prepare the Fe-based biochar is a kind of modification method to improve Cr⁶⁺ removal capacity of original biochar (Dong et al., 2021; Sun et al., 2023). The Fe-based compounds can participate in Cr⁶⁺ removal by reduction (Zhang et al., 2023; Sahu et al., 2022). Besides, the Fe-based biochar can be quickly recycled from wastewater under extra filed. Yan et al. (2023)

modified biochar with chitosan for Cr⁶⁺ removal with adsorption amount of 125.34 mg g⁻¹ (Yan et al., 2023). Chu et al. (2023) modified the Fe@CSBC by loading Fe₃O₄ on biochar derived from corn straw, which is used for capturing Cr⁶⁺ in wastewater with adsorption amount of 138.8 mg g⁻¹ (Chu and Nguyen, 2023). Qiu et al. (2020) prepared nano-zero-valent iron/sludge-derived biochar for Cr⁶⁺ adsorption and reduction with 64.13 mg g⁻¹ (Qiu et al., 2020). Wang et al. (2020) used magnetic greigite/biochar composites to remove Cr⁶⁺ with removal of 93 % by adsorption and reduction (Wang et al., 2020). However, the preparation methods of the Fe-based biochar are more or less environmentally unstable and complicated to synthesize, which limits their practical application. It should be developed the simple and low-cost method for preparation of the Fe-based biochar overcome these disadvantages. FeCl₃ is a kind of the chemical activation agent, which can improve the pore structure of biochar (Wang et al., 2020). FeCl₃ can generate the Fe₃O₄ on biochar after heat.

In this work, magnetic biochar is successfully prepared by pyrolysis of waste wooden building formwork using FeCl₃ as chemical agent for Cr⁶⁺ wastewater purification. The magnetic biochar is characterized to analyze its physicochemical properties. Cr⁶⁺ removal capacity of magnetic biochar is also investigated. The objectives of this work are: (1) to analyze physicochemical properties of the magnetic biochar, (2) to investigate Cr⁶⁺ adsorption performance of magnetic biochar, (3) to explore possible involved Cr⁶⁺ removal mechanism, (4) to investigate Cr⁶⁺ removal capacity in column adsorption experiment.

2. Experimental section

2.1. Material

The waste wooden building formwork is collected from local construction site, which is crushed with the particle size of the 2 mm. The FeCl₃ is obtained from Sinopharm Chemical Reagent Co China. Potassium dichromate (K₂Cr₂O₇) is purchased from the Yantai Shuangshuang Chemical Co., Ltd, China.

2.2. Synthesis of the magnetic biochar

Waste wooden building formwork is mixed with 20 g FeCl₃ in the aqueous solution, which is stirred for 24 h. Subsequently, mixture is dried using electric dry oven at the temperature of 80 °C for 24 h. Finally, dried mixture is heated at 400–600 °C for 30 min in the microwave furnace under nitrogen atmosphere with nitrogen flow rate of 200 mL/min. Finally, the residue in the microwave furnace is named as the MB-400 °C, MB-500 °C and MB-600 °C.

2.3. Adsorption experiment

The influence of the pH on Cr⁶⁺ adsorption is investigated at pH of 2–7. The adsorption isotherm experiments are carried out as follows. 0.1 g magnetic biochar is mixed with 100 mL Cr⁶⁺ solution with different concentration, which is stirred using the magnetic stirrer with a shaking speed of 300 r/min (pH=2). The adsorption time is 24 h to reach the adsorption equilibrium. Mixture solution is sampled to detect the residue concentration after adsorption equilibrium. After adsorption, the adsorbent and the adsorbed solution are separated by filtration using a 0.22 μm filter. Cr⁶⁺ concentration is obtained using UV–VIS spectroscopy at 540 nm. Cr⁶⁺ adsorption amounts (q_e and q_d) in the adsorption experiment are calculated from the following equation. Cr⁶⁺ adsorption behavior on MB-600 °C is investigated by Langmuir, Freundlich, and Hill models, which are described in the Table S1.

The experiment method of the adsorption kinetics is similar with the adsorption isotherm. Pseudo-first/second order and Intraparticle diffusion models are used to explain the Cr⁶⁺ adsorption kinetics process, which are presented in Table S2.

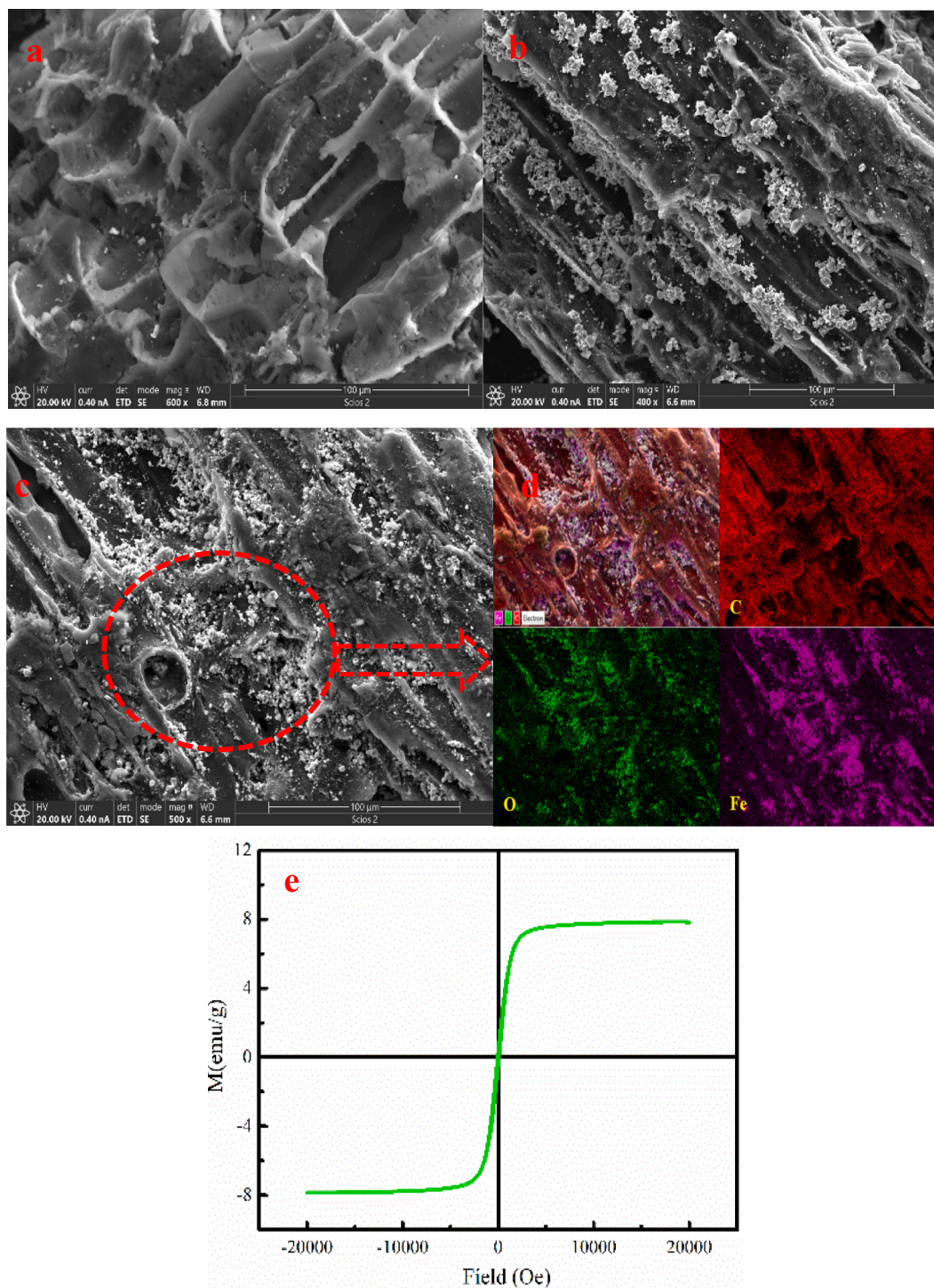


Fig. 3. The microstructure analysis of the MB-600 °C (a-d) and the hysteresis loop of the MB-600 °C (e).

$$q_t = \frac{V(C_0 - C_t)}{M} \quad (1)$$

$$q_e = \frac{V(C_0 - C_e)}{M} \quad (2)$$

q_t , adsorption amount of Cr^{6+} adsorbed over time, mg/g.

q_e , Cr^{6+} adsorption amount, mg/g.

C_0 , initial Cr^{6+} concentration, mg/L.

C_t , Cr^{6+} concentration over time, mg/L.

C_e , Cr^{6+} equilibrium concentration, mg/L.

M , quality of the magnetic biochar, g.

V , solution volume, L.

2.4. Characterization

The specific surface area of magnetic biochar is analyzed using the Brunauer Emmett Teller (BET) method using the Autosorb instrument. The surface properties of magnetic biochar are analyzed by the X-ray photoelectron spectroscopy (XPS). The surface chemical composition is investigated using the X-ray diffractometer (XRD). Scanning electron microscopy (SEM) is used to analyze the surface morphologies of magnetic biochar. The chemical functional groups of samples are analyzed

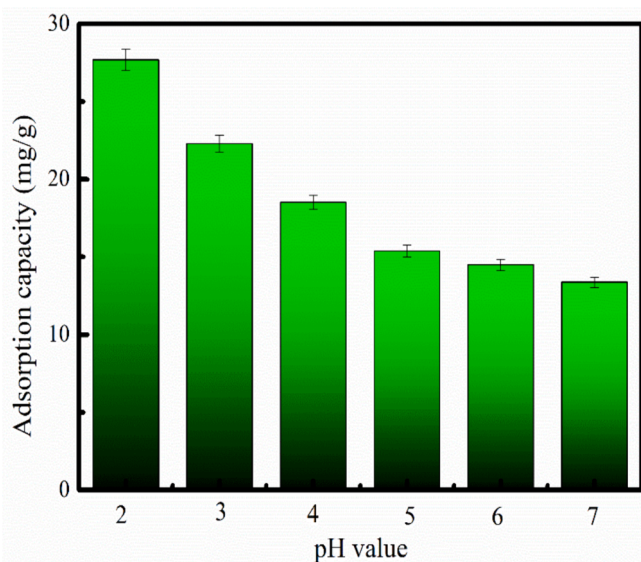


Fig. 4. Influence of the solution of the pH on Cr⁶⁺ adsorption.

using the Fourier transform infrared spectroscopy (FTIR). Zeta potential measurements are conducted using a ZetaPALS.

3. Results and discussions

3.1. Characterization analysis

Fig. 1 shows the XRD analysis of magnetic biochar. The characteristic peaks of the Fe₃O₄ ($2\theta = 18.23^\circ, 30.01^\circ, 35.4^\circ, 43.04^\circ, 56.89^\circ, 51.8^\circ$ and 62.51°) are appeared in the magnetic biochar with good crystallinity. This result indicates that FeCl₃ is converted into the Fe₃O₄ at temperature of the 400–600 °C. It also means that the magnetic biochar has magnetic, which can be quickly recycled from Cr⁶⁺ wastewater due to existence of the Fe₃O₄.

Fig. 2 shows the N₂-adsorption isotherm of the magnetic biochar. The pore structure parameter of the magnetic biochar is presented in Table 1. As Fig. 2 shown, N₂ adsorption amount of the magnetic biochar significantly increases at P/P₀ < 0.1, and then the curve tends to slowly increase. “Hysteresis loop” appears on magnetic biochar, indicating the mesoporous structure of magnetic biochar. As Table 1 shown, the MB-600 °C has large surface area, which is acted as the candidate of the magnetic biochar for further investigation.

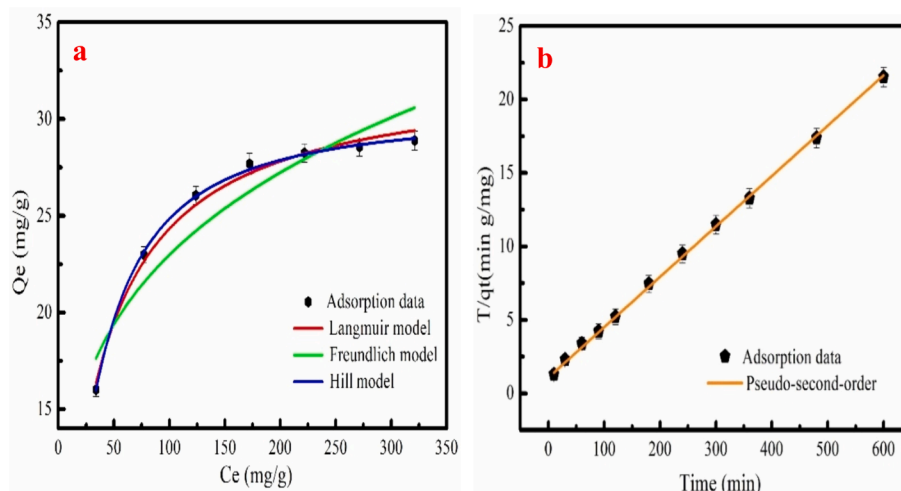


Fig. 5. The Cr⁶⁺ adsorption data fitting the adsorption isotherm models (a) and The Cr⁶⁺ adsorption data fitting Pseudo-second-order equation (b).

The microstructure analysis of the MB-600 °C is shown in the Fig. 3a-d. As Fig. 3a-b shown, MB-600 °C has developed pore structure. Besides, the surface of the MB-600 °C has gray particulate matter. EDS mapping image analysis result indicates that C, O and Fe are found on MB-600 °C (Fig. 3c-d). The gray particulate matter on the MB-600 °C is the Fe₃O₄ combined with XRD analysis.

Fig. 3e shows the hysteresis loop analysis of the MB-600 °C. As Fig. 3e shown, the saturation magnetization of the MB-600 °C is 7.85 emu/g, indicating that MB-600 °C has certain of the soft magnetic property. The MB-600 °C can be quickly separated and recovered from aqueous solution under the action of applied magnetic field (Fig.S1). As Fig.S1 shown, the MB-600 °C is gathered on the wall of the bottle under the action of applied magnetic field, which is consistent with the hysteresis loop analysis.

Table 2

The calculated results of adsorption isotherm models.

Isotherm models	Models Parameter	Fitting result Cr ⁶⁺
Langmuir	q _m (mg/g)	32.47
	K _L (L/mg)	0.0299
	R ²	0.9927
Freundlich	1/n	0.2453
	K _F ((mg/g).(L/mg) ^{1/n})	7.42
	R ²	0.90083
Hill	Q _m	30.41
	n	1.28
	K	31.49
	R ²	0.9990

Table 3

The calculated results of adsorption kinetics models.

Isotherm models	Models Parameter	Fitting result Cr ⁶⁺
Pseudo-first order	q _{e,cal} (mg/g)	25.21
	K ₁ (1/min)	0.028
	R ²	0.9448
Pseudo-second order	q _{e,cal} (mg/L)	29.17
	K ₂ (g/mg min)	1.077
	R ²	0.9989
Intraparticle diffusion	C ₁	1.32
	K ₃₁ (mg/g min ^{1/2})	2.07
	R ²	0.9944
	C ₂	19.91
	K ₃₂ (mg/g min ^{1/2})	0.35
R ²	0.8976	

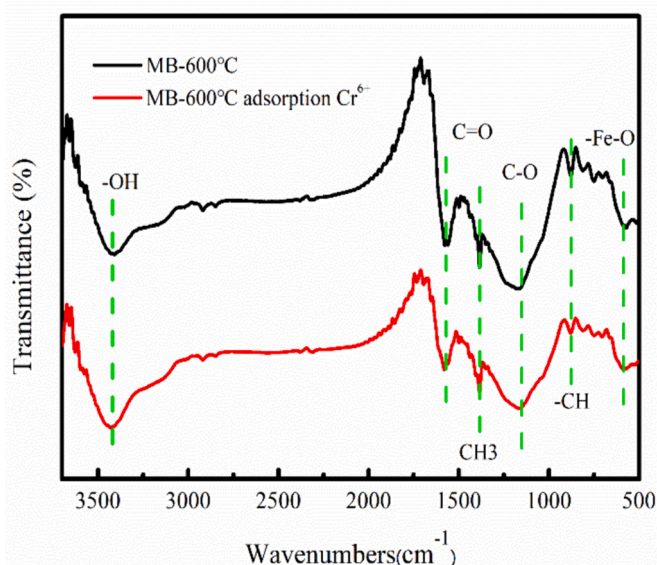


Fig. 6. FT-IR spectra of MB-600 °C before and after Cr⁶⁺ adsorption.

3.2. Influence of pH

Cr⁶⁺ has various of forms at different pH (Asoubar et al., 2023). Fig. 4 presents Cr⁶⁺ adsorption behavior on MB-600 °C at pH of 2–7. Fig. 4 shows that MB-600 °C has large Cr⁶⁺ adsorption amount at pH of 2–4. There exists lots of H⁺ in the aqueous solution, which makes MB-600 °C have positive charge. Therefore, MB-600 °C can adsorb Cr⁶⁺ by electrostatic adsorption. The H⁺ concentration is general decrease as pH increases. Therefore, Cr⁶⁺ adsorbing amount is generally decrease with increasing in pH. The zeta potential value of the MB-600 °C is about 5.2 (Fig.S2). This result indicates that MB-600 °C has positive potential at pH<5.2, and becomes negative potential at pH>5.2. The MB-600 °C has large Cr⁶⁺ adsorption amount at pH=2. Therefore, the desire pH for MB-600 °C adsorption Cr⁶⁺ is 2.

3.3. Adsorption isotherms investigation

The Cr⁶⁺ adsorption behavior on MB-600 °C is investigated by Langmuir, Freundlich, and Hill models. Fig. 5a shows the Cr⁶⁺ adsorption data fitting adsorption isotherm equations, and fitting parameters are listed in Table.2. As Table 2 shown, compared with Freundlich model, the R² value of Cr⁶⁺ adsorption data fitting the Langmuir/Hill equation has large R². Cr⁶⁺ adsorption amount obtained from Hill model is 30.41 mg/g. The parameter (K_L) of Langmuir model is used to calculate the dimensionless factor R_L that can investigate feasible of Cr⁶⁺ adsorption on MB-600 °C (Cheng et al., 2021). Calculated method is in the following equation.

$$R_L = \frac{1}{1 + K_L C_0} \quad (3)$$

If the R_L belongs to 0–1, Cr⁶⁺ adsorption process is feasible. R_L values of Cr⁶⁺ adsorption on MB-600 °C is 0.0872–0.4009, indicating that MB-600 °C is feasible for Cr⁶⁺ adsorption. Besides, the values of the heterogeneity (1/n) calculated from Freundlich that can represent the bond distribution (Tang et al., 2018). The 1/n value of Cr⁶⁺ adsorption on MB-600 °C is 0.2453, which is less than 1. This result confirms that Cr⁶⁺ adsorption process is feasible and favorable (Xiang et al., 2019).

The Cr⁶⁺ adsorption amounts of other adsorbents are also compared with MB-600 °C (Table S3). Cr⁶⁺ adsorption amount of MB-600 °C is larger than that reported adsorbents. These results prove that the MB-600 °C is the promising adsorbent for Cr⁶⁺ wastewater purification.

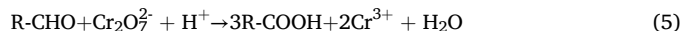
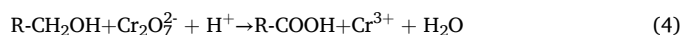
3.4. Adsorption kinetics investigation

The Cr⁶⁺ adsorption data is analyzed by the Pseudo-first/second order and Intraparticle diffusion equations. The calculated results are listed in Table 3. Correlation coefficient (R²) value of Cr⁶⁺ adsorption process fitting Pseudo-second order is 0.9989, which is higher than other adsorption kinetics models (Table 3). Thus, Pseudo-second order is better to describe Cr⁶⁺ adsorption kinetic process, indicating that chemical adsorption influences Cr⁶⁺ adsorption (Cheng et al., 2022). Fig. 5b shows Cr⁶⁺ adsorption data fitting Pseudo-second-order equation. The Intraparticle diffusion fitting result has two stages (Fig.S3). The C₁ and C₂ value of Cr⁶⁺ calculated from Intraparticle diffusion model are 1.32 and 19.91, respectively. The calculated C value isn't zero, indicating that Cr⁶⁺ adsorption on MB-600 °C isn't alone controlled by Intraparticle diffusion.

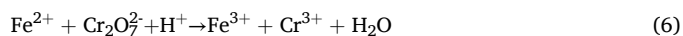
3.5. Removal mechanism

The zeta potential of the MB-600 °C is about 5.2. The surface potential of the MB-600 °C is positive charge at pH of 2. Therefore, MB-600 °C can adsorb Cr⁶⁺ by electrostatic attraction. As Fig. 6 shown, MB-600 °C has the OH, C=O, C-O and Fe-O group, demonstrating that MB-600 °C has abundant functional group. Besides, the oxygen-containing functional groups can easily obtain the protons at pH of 2 (Liang et al., 2023). The oxygen-containing functional groups can be used as the electron donor, contributing to Cr⁶⁺ removal by adsorption/reduction (Singh et al., 2022; Zhao et al., 2024). After Cr⁶⁺ adsorption, the peak intensity and peak location of oxygen containing functional groups have changed, indicating that these groups involve in Cr⁶⁺ removal. Fe²⁺ comes from the dissolution of Fe₃O₄, which might be an important reaction pathway for Cr⁶⁺ removal by reduction (Zhao et al., 2024).

Fig. 7a-b shows the C 1 s peaks of MB-600 °C before and after Cr⁶⁺ adsorption. The peaks at 288.58, 285.21 and 284.60 eV are C=O, C-O and C-C group, respectively (Tang et al., 2021; Wang et al., 2020). For MB-600 °C, upon reaction with Cr⁶⁺, the C-O percentage decreases from 35.29 % to 28.27 %, which indicates that -CHO is an electron donor that is oxidized into -COOH by Cr⁶⁺ (Zhang et al., 2020). Generally, the C-O group is the adsorption and reduction site of the MB-600 °C, and adsorption and reduction occur simultaneously (Liu et al., 2023) (Eq.4). However, C=O proportion decreases, which maybe C=O involves in Cr⁶⁺ removal (Eq.5) (Mutabazi et al., 2024).



As Fig. 7c shown, the two peaks of Cr 2p_{1/2} and Cr 2p_{3/2} correspond to the 587.24 eV and 577.04 eV, respectively. The peaks at 576.89 eV and 586.80 eV indicate the presence of Cr³⁺, suggesting that Cr⁶⁺ is partially reduced into Cr³⁺ (Luo et al., 2021). Fig. 7c-d shows the Fe 2p spectra of the MB-600 °C before and after Cr⁶⁺ adsorption, which can be divided in four peaks. The peaks at 710.85 eV and 724.21 eV correspond to Fe²⁺, while Fe³⁺ appears at peaks of 712.74 eV and 725.98 eV. Peak area ratio of Fe²⁺/Fe³⁺ decreases by 0.37 after Cr⁶⁺ adsorption, implying that the dissolved Fe²⁺ involves in Cr⁶⁺ reduction process. The analysis result is consistent with Cr2p spectrum analysis. The Fe²⁺ is reducing substances, which can reduce Cr₂O₇²⁻ into Cr³⁺ (Eq.6) (Li et al., 2019).



Furthermore, MB-600 °C can also realize Cr⁶⁺ removal by the pore filling (Su et al., 2022; Yang et al., 2020). The MB-600 °C shows flourishing pore structure that plays a vital role in Cr⁶⁺ removal process. The summary of Cr⁶⁺ adsorption mechanism is shown in the Fig. 8.

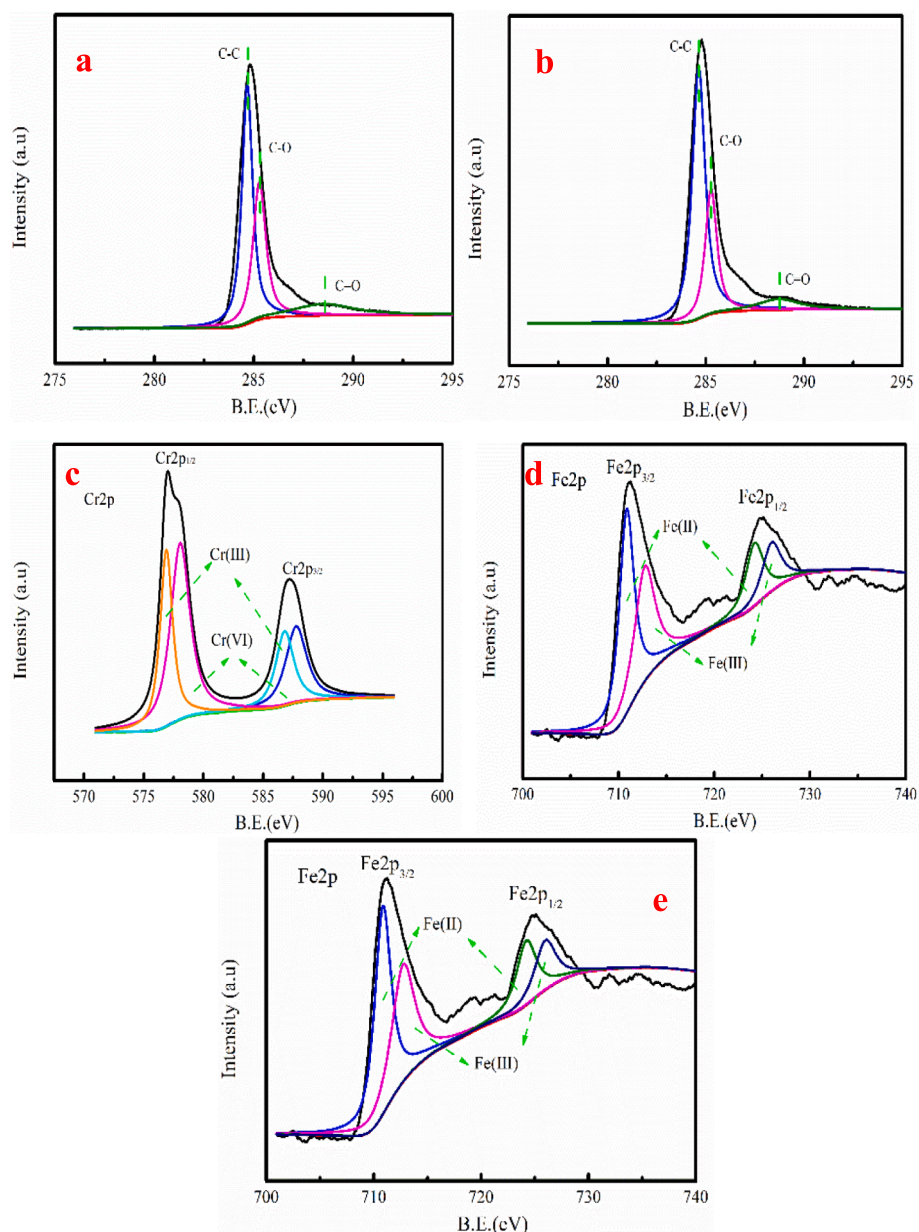


Fig. 7. The detail survey of the C1s before (a) and after Cr^{6+} adsorption (b), detail survey of the Cr2p after adsorption Cr^{6+} (c) and detail survey of the Fe2p after adsorption Cr^{6+} (d-e).

3.6. Reusability investigation

Fig.S4 shows reusability results of MB-600 °C. As Fig.S4 shown, the Cr^{6+} adsorption capability of MB-600 °C decreases as cycle number increases. The Cr^{6+} adsorption amount is dropped to 19.84 mg/g after three cycles, which decreases by 28.32 %. The reason is that part of active sites of MB-600 °C loses adsorption capacity after regeneration. MB-600 °C still shows large Cr^{6+} adsorption capacity after regeneration, which has practical application potential in Cr^{6+} wastewater purification.

3.7. Effect of Fe^{2+}

The Fe 2p spectra analysis of the MB-600 °C before and after Cr^{6+} adsorption indicates that Fe^{2+} involves in Cr^{6+} removal. Besides, the electron transfer occurs between Fe^{2+} and Cr^{6+} . Fe_3O_4 can dissolve to generate Fe^{2+} because the pH of Cr^{6+} adsorption solution is 2. This result indicates that the Fe^{2+} exists adsorption solution and participates in

Cr^{6+} reduction. Fe^{2+} is an important reductant with a low standard electrode potential of 0.77 V/SHE and can transform Cr^{6+} to Cr^{3+} ($\text{E}(\text{HCrO}_4/\text{Cr}^{3+}) = 1.35 \text{ V/SHE}$) (Jiang et al., 2019). Therefore, the influence of Fe^{2+} on Cr^{6+} removal is analyzed in existence of 1,10-phenanthroline that make Fe^{2+} cannot participate in Cr^{6+} removal (Liu et al., 2019). As Fig. 9a shown, the Cr^{6+} removal is decrease in existence of the 1,10-phenanthroline compared to without adding 1,10-phenanthroline. The analysis result demonstrates that Fe^{2+} participates in Cr^{6+} removal.

As Fig. 9b shown, the total Cr and Cr^{6+} concentration rapidly decrease with increasing in adsorption time without adding 1,10-phenanthroline. The total Cr concentration is gradual decrease and Cr^{3+} concentration exhibits an increasing trend, indicating that Cr^{6+} adsorption and reduction simultaneously occur. While, Cr^{3+} concentration increases as time continues to increase. However, Cr^{3+} concentration gradually decreases as adsorption time continues to increase, indicating that part of Cr^{3+} is adsorbed on MB-600 °C. The equation of Fe^{2+} involves in Cr^{6+} removal is listed in Eq. (6). Cr^{6+} removal by MB-600 °C is restrained in existence of 1,10-phenanthroline, demonstrating

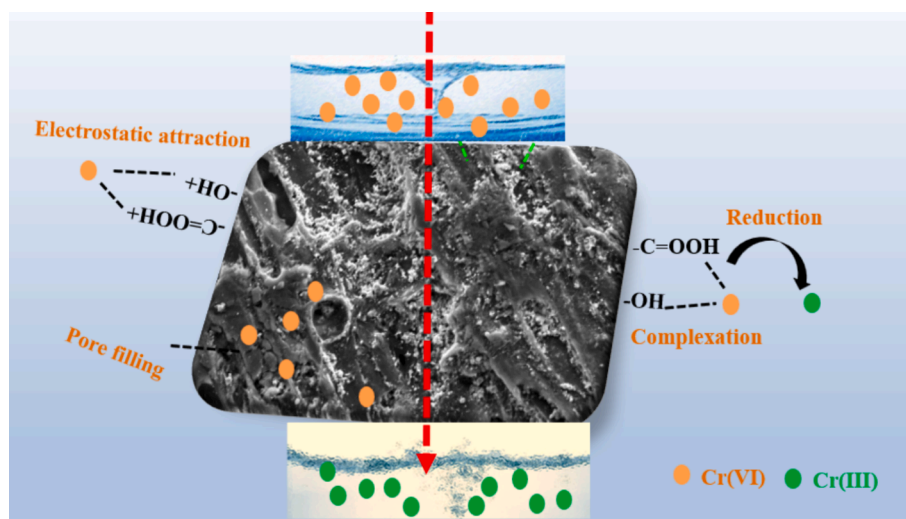


Fig. 8. The summary of Cr^{6+} adsorption mechanism.

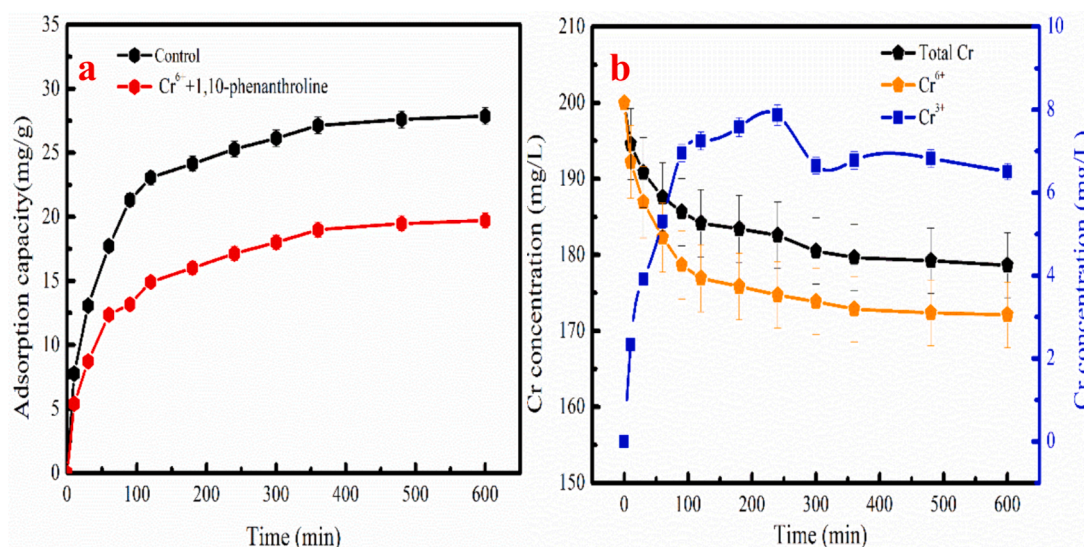


Fig. 9. The influence of 1,10-phenanthroline on Cr^{6+} removal(a), the total Cr, Cr^{6+} , and Cr^{3+} concentration in the Cr removal process(b).

that Fe^{2+} plays an important role in Cr^{6+} removal.

3.8. Explore using DFT calculations

Combined with the results of XPS and FTIR, it could be found that the oxygen-containing functional group on the MB-600 °C mainly included hydroxyl, COOH, -OH and Fe-O groups. Thus, the MB-600 °C model with various oxygen-containing functional groups is constructed (Cheng et al., 2021). Binding energies of the COOH, -OH and Fe-O groups interactions with Cr^{6+} are calculated using DFT. Fig. S5 shows the calculated result. According to the calculation result in the Fig.S5, it exists energy barrier in Cr^{6+} adsorption process. Compared with the binding energies of Cr^{6+} interactions with -OH and -COOH group, the -Fe-O group is more negative. The analysis data demonstrates that -Fe-O group plays a critical role in Cr^{6+} removal by surface complexation.

3.9. Column adsorption

Thomas and Yoon-Nelson equation are employed for Cr^{6+} adsorption process using fixed-bed adsorption (Table S4). The fitting analysis results are presented in Table S5. As Table S5 shown, Cr^{6+} breakthrough

curves can be analyzed using the Thomas and Yoon-Nelson equation with high R^2 . Yoon-Nelson equation is better to describe Cr^{6+} adsorption process because of large R^2 . According to Thomas equation calculation, Cr^{6+} adsorption amount of the MB-600 °C is 56.64 mg/g. It demonstrates that MB-600 °C has enormous potential in governing environmental concerns of wastewater. Fig.S6 presents breakthrough curve of Cr^{6+} adsorption on MB-600 °C.

3.10. Economic feasibility

Preparation cost of the MB-600 °C is very important parameter for actual application on an industrial scale. According to previous literature, the total production cost of MB-600 °C is presented in Table S6 (Jiang et al., 2019). As Table S6 shown, the approximate preparation cost is about \$2.48 for 1 kg MB-600 °C. However, production cost of 100 mesh activated carbon is estimated as \$ 40/1kg. Compared with commercial activated carbon, the production cost of MB-600 °C is cheap. Cr^{6+} adsorption amount of activated carbon and nZVI/sewage sludge co-pyrolyzed magnetic biochar are 23.35 and 13.27 mg/g, respectively (Mutabazi et al., 2024; Liu et al., 2020). Estimated treatment cost of 1 Kg Cr^{6+} is \$ 81.55 for MB-600 °C. Compared with the above adsorbent, the

estimated treatment cost of the 1 Kg Cr⁶⁺ is cheap. Therefore, MB-600 °C can be acted as low-cost adsorbent for Cr⁶⁺ removal.

4. Conclusions

The magnetic biochar is successfully prepared using the simple one-step pyrolysis method for Cr⁶⁺ removal from wastewater. The Cr⁶⁺ adsorption capacity is 30.41 mg/g at pH=2. The electrostatic attraction, surface complexation, reduction and pore filling are responsible for Cr⁶⁺ removal, based on mechanism analysis. Existence of Fe²⁺ contributes to Cr⁶⁺ removal by reduction in aqueous solution. The –Fe-O group is important in Cr⁶⁺ removal process compared to –COOH and –OH groups based on DFT calculation. The magnetic biochar has large column adsorption amount of 56.64 mg/g. The production cost of the magnetic biochar is about \$2.48/1kg, based on preliminary economic analysis.

CRedit authorship contribution statement

Chao Lv: Resources, Methodology, Investigation, Formal analysis, Conceptualization. **Peng Liu:** Writing – original draft, Supervision, Methodology, Investigation, Funding acquisition.

Declaration of competing interest

The authors declare that they have no known competing financial interests or personal relationships that could have appeared to influence the work reported in this paper.

Acknowledgments

The authors would like to express their gratitude to the Ph.D. Research Start-up Funding Project of Panzhuhua University (XJ2022001301), and Panzhuhua Directed Science and Technology Planning Projects (2022ZD-G-4) for financial support.

Appendix A. Supplementary material

Supplementary data to this article can be found online at <https://doi.org/10.1016/j.arabjc.2024.105943>.

References

- Amin, M., Chetpattananondh, P., 2019. Biochar from extracted marine *Chlorella* sp. residue for high efficiency adsorption with ultrasonication to remove Cr(VI), Zn(II) and Ni(II). *Bioresour. Technol.* 289, 121578.
- Asoubar, S., Mehrizad, A., Behnajady, M.A.A., Ramazani, M.E., Gharbani, P., 2023. Hexavalent chromium reduction and Rhodamine B degradation by visible-light-driven photocatalyst of stannum indium sulfide-samarium vanadate. *npj Clean Water* 6, 213411.
- Cai, Y., Ran, Z., Cang, Y., Chen, X., Shaaban, M., Peng, Q.A., 2023. Efficient removal of Cr(VI) and As(V) from an aquatic system using iron oxide supported typha biochar. *Environ. Res.* 225, 115588.
- Cheng, S., Xing, B., Shi, C., Nie, Y., Xia, H., 2021. Efficient and selective removal of Pb(II) from aqueous solution by modification crofton weed: Experiment and density functional theory calculation. *J. Clean. Prod.* 280.
- Cheng, S., Xing, B., Shi, C., Nie, Y., Xia, H., 2021. Efficient and selective removal of Pb(II) from aqueous solution by modification crofton weed: Experiment and density functional theory calculation. *J. Clean. Prod.* 280, 124407.
- Cheng, S., Zhao, S., Guo, H., Xing, B., Liu, Y., Zhang, C., Ma, M., 2022. High-efficiency removal of lead/cadmium from wastewater by MgO modified biochar derived from crofton weed. *Bioresour. Technol.* 343, 126081.
- Chu, T.T.H., Nguyen, M.V., 2023. Improved Cr(VI) adsorption performance in wastewater and groundwater by synthesized magnetic adsorbent derived from Fe₃O₄ loaded corn straw biochar. *Environ. Res.* 216, 114764.
- Dong, F.X., Yan, L., Zhou, X.H., Huang, S.T., Liang, J.Y., Zhang, W.X., Guo, Z.W., Guo, P. R., Qian, W., Kong, L.J., Chu, W., Diao, Z.H., 2021. Simultaneous adsorption of Cr(VI) and phenol by biochar-based iron oxide composites in water: Performance, kinetics and mechanism. *J. Hazard. Mater.* 416, 125930.
- Fu, F., Wang, Q., 2011. Removal of heavy metal ions from wastewaters: A review. *J. Environ. Manage.* 92, 407–418.
- Guo, H., Cheng, S., Xing, B., Meng, M., Feng, L., Nie, Y., Zhang, C., 2024. Preparation of three kinds of efficient sludge-derived adsorbents for metal ions and organic wastewater purification. *Arab. J. Chem.* 17, 105671.
- Hong, X., Ding, C., Shi, M., Ding, Z., Du, P., Xia, M., Wang, F., 2024. Easy separation dual-function Cu₂O@LDH@Fe₃O₄ adsorbent for the removal of Cr(VI) under dark conditions: Experimental and mechanistic study. *Sep. Purif. Technol.* 332, 125734.
- Jiang, B., Gong, Y., Gao, J., Sun, T., Liu, Y., Oturan, N., Oturan, M.A., 2019. The reduction of Cr(VI) to Cr(III) mediated by environmentally relevant carboxylic acids: State-of-the-art and perspectives. *J. Hazard. Mater.* 365, 205–226.
- Li, Y., Chen, X., Liu, L., Liu, P., Zhou, Z., Huhetaoli, Y., Wu, T.L., 2022. Characteristics and adsorption of Cr(VI) of biochar pyrolyzed from landfill leachate sludge. *J. Anal. Appl. Pyrol.* 162, 105449.
- Li, J., Lan, H., Liu, H., Zhang, G., An, X., Liu, R., Qu, J., 2019. Intercalation of nanosized Fe₃C in iron/carbon to construct multifunctional interface with reduction, catalysis, corrosion resistance, and immobilization capabilities. *ACS Appl. Mater. Interfaces* 11, 15709–15717.
- Liang, J.Y., Zhang, W.X., Yao, X.W., Chen, M.L., Chen, X., Kong, L.J., Diao, Z.H., 2023. New insights into co-adsorption of Cr⁶⁺ and chlortetracycline by a new fruit peel based biochar composite from water: Behavior and mechanism. *Colloids Surf. A Physicochem. Eng. Asp.* 672, 131764.
- Liu, L., Liu, X., Wang, D., Lin, H., Huang, L., 2020. Removal and reduction of Cr(VI) in simulated wastewater using magnetic biochar prepared by co-pyrolysis of nano-valent iron and sewage sludge. *J. Clean. Prod.* 257, 120562.
- Liu, P., Wang, X., Ma, J., Liu, H., Ning, P., 2019. Highly efficient immobilization of NZVI onto bio-inspired reagents functionalized polyacrylonitrile membrane for Cr(VI) reduction. *Chemosphere* 220, 1003–1013.
- Liu, K., Zhao, D., Hu, Z., Xiao, Y., He, C., Jiang, F., Zhao, N., Zhao, C., Zhang, W., Qiu, R., 2023. The adsorption and reduction of anionic Cr(VI) in groundwater by novel iron carbide loaded on N-doped carbon nanotubes: Effects of Fe-confinement. *Chem. Eng. J.* 452, 139357.
- Luo, Q., Huang, X., Luo, Y., Yuan, H., Ren, T., Li, X., Xu, D., Guo, X., Wu, Y., 2021. Fluorescent chitosan-based hydrogel incorporating titanate and cellulose nanofibers modified with carbon dots for adsorption and detection of Cr(VI). *Chem. Eng. J.* 407, 127050.
- Mao, P., Yang, X., Wang, Z., Ping, X., Tian, Y., Chen, Y., Chen, Z., Zhang, J., Shen, J., Sun, A., 2024. Interfacial engineering of 0D/2D Cd_{0.5}Zn_{0.5}S/Ti₃C₂ for efficient photocatalytic synergistic removal of antibiotics and Cr(VI). *J. Environ. Chem. Eng.* 12, 111649.
- Mutabazi, E., Qiu, X., Song, Y., Li, C., Jia, X., Hakizimana, I., Niu, J., Nuramkhaan, M., Zhao, Y., 2024. Cr(VI) adsorption on activated carbon, sludge derived biochar, and peanut shells derived biochar: Performance, mechanisms during the reuse process and site energy distribution analysis. *J. Water Process Eng.* 57, 104679.
- Qin, X., Cheng, S., Xing, B., Qu, X., Shi, C., Meng, W., Zhang, C., Xia, H., 2023. Preparation of pyrolysis products by catalytic pyrolysis of poplar: Application of biochar in antibiotic wastewater treatment. *Chemosphere* 338, 139519.
- Qiu, Y., Zhang, Q., Gao, B., Li, M., Fan, Z., Sang, W., Hao, H., Wei, X., 2020. Removal mechanisms of Cr(VI) and Cr(III) by biochar supported nanosized zero-valent iron: Synergy of adsorption, reduction and transformation. *Environ. Pollut.* 265, 115018.
- Qu, J., Zhang, W., Bi, F., Yan, S., Miao, X., Zhang, B., Wang, Y., Ge, C., Zhang, Y., 2022. Two-step ball milling-assisted synthesis of N-doped biochar loaded with ferrous sulfide for enhanced adsorptive removal of Cr(VI) and tetracycline from water. *Environ. Pollut.* 306, 119398.
- Sahu, U.K., Ji, W., Liang, Y., Ma, H., Pu, S., 2022. Mechanism enhanced active biochar support magnetic nano zero-valent iron for efficient removal of Cr(VI) from simulated polluted water. *J. Environ. Chem. Eng.* 10, 107077.
- S. Singh, A.G. Anil, T.S.S.K. Naik, B. U. S. Khasnabis, B. Nath, V. Kumar, S. Subramanian, J. Singh, P.C. Ramamurthy, Mechanism and kinetics of Cr(VI) adsorption on biochar derived from *Citrobacter freundii* under different pyrolysis temperatures, *Journal of Water Process Engineering*, 47 (2022) 102723.
- Su, Y., Shi, Y., Jiang, M., Chen, S., 2022. One-step synthesis of nitrogen-doped porous biochar based on N-doping Co-activation method and its application in water pollutants control. *Int. J. Mol. Sci.* 23.
- Sun, Y., Lyu, H., Gai, L., Sun, P., Shen, B., Tang, J., 2023. Biochar-anchored low-cost natural iron-based composites for durable hexavalent chromium removal. *Chem. Eng. J.* 476, 146604.
- Tang, L., Yu, J., Pang, Y., Zeng, G., Deng, Y., Wang, J., Ren, X., Ye, S., Peng, B., Feng, H., 2018. Sustainable efficient adsorbent: Alkali-acid modified magnetic biochar derived from sewage sludge for aqueous organic contaminant removal. *Chem. Eng. J.* 336, 160–169.
- Tang, J., Zhao, B., Lyu, H., Li, D., 2021. Development of a novel pyrite/biochar composite (BM-FeS₂@BC) by ball milling for aqueous Cr(VI) removal and its mechanisms. *J. Hazard. Mater.* 413, 125415.
- Wang, X., Xie, Y., Chen, X., Zhou, X., Hu, W., Li, P., Li, Y., Zhang, Y., Wang, Y., 2020. A novel g-C₃N₄ modified biosynthetic Fe(III)-hydroxysulfate for efficient photoreduction of Cr(VI) in wastewater treatment under visible light irradiation. *Chem. Eng. J.* 398, 125632.
- Wang, X., Xu, J., Liu, J., Liu, J., Xia, F., Wang, C., Dahlgren, R.A., Liu, W., 2020. Mechanism of Cr(VI) removal by magnetic greigite/biochar composites. *Sci. Total Environ.* 700, 134414.
- Wang, Y., Yang, Q., Chen, J., Yang, J., Zhang, Y., Chen, Y., Li, X., Du, W., Liang, A., Ho, S.-H., 2020. Adsorption behavior of Cr(VI) by magnetically modified *Enteromorpha prolifera* based biochar and the toxicity analysis. *J. Hazard. Mater.* 395, 122658.
- Xiang, Y., Xu, Z., Zhou, Y., Wei, Y., Long, X., He, Y., Zhi, D., Yang, J., Luo, L., 2019. A sustainable ferromanganese biochar adsorbent for effective levofloxacin removal from aqueous medium. *Chemosphere* 237, 124464.
- Xiao, H., Liang, L., Peng, H., Fang, D., Wu, G., Wang, Y., Zhu, Y., Zeng, Z., 2024. Can Cr(VI) and tetracycline be simultaneously removed by stabilized FeS nanoparticles via aeration at circumneutral conditions? *J. Water Process Eng.* 60, 105146.

- Yan, L., Guo, W., Huang, B., Chen, Y., Ren, X., Shen, Y., Zhou, Y., Cheng, R., Zhang, J., Qiu, M., Hu, B., 2023. Efficient removal of Cr(VI) by the modified biochar with chitosan schiff base and MnFe₂O₄ nanoparticles: Adsorption and mechanism analysis. *J. Environ. Chem. Eng.* 11, 109432.
- Yang, Q., Wu, P., Liu, J., Rehman, S., Ahmed, Z., Ruan, B., Zhu, N., 2020. Batch interaction of emerging tetracycline contaminant with novel phosphoric acid activated corn straw porous carbon: Adsorption rate and nature of mechanism. *Environ. Res.* 181, 108899.
- Zhang, T., Bai, W., Dong, Q., Chu, D., Wang, L., He, Y., 2023. Hydrodynamic analysis of carbon nanotube clusters in distributor-less conical fluidized beds with step-by-step scaling. *Chin. J. Chem. Eng.*
- Zhang, Y., Liu, N., Yang, Y., Li, J., Wang, S., Lv, J., Tang, R., 2020. Novel carbothermal synthesis of Fe, N co-doped oak wood biochar (Fe/N-OB) for fast and effective Cr(VI) removal. *Colloids Surf. A Physicochem. Eng. Asp.* 600, 124926.
- Zhao, X., Liu, M., Feng, H., Luo, X., Yang, Y., Hu, J., Hu, Y., 2024. Effects and mechanisms on Cr(VI) and methylene blue adsorption by acid (NH₄)₂S₂O₈ modified sludge biochar. *Sep. Purif. Technol.* 345, 127100.
- Zhao, N., Zhao, C., Tsang, D.C.W., Liu, K., Zhu, L., Zhang, W., Zhang, J., Tang, Y., Qiu, R., 2021. Microscopic mechanism about the selective adsorption of Cr(VI) from salt solution on O-rich and N-rich biochars. *J. Hazard. Mater.* 404, 124162.
- Zou, H., Zhao, J., He, F., Zhong, Z., Huang, J., Zheng, Y., Zhang, Y., Yang, Y., Yu, F., Bashir, M.A., Gao, B., 2021. Ball milling biochar iron oxide composites for the removal of chromium (Cr(VI)) from water: Performance and mechanisms. *J. Hazard. Mater.* 413, 125252.